AIP Applied Physics Letters

Time-resolved analysis of thickness-dependent dewetting and ablation of silver films upon nanosecond laser irradiation

Dongfeng Qi, Dongwoo Paeng, Junyeob Yeo, Eunpa Kim, Letian Wang, Songyan Chen, and Costas P. Grigoropoulos

Citation: Applied Physics Letters **108**, 211602 (2016); doi: 10.1063/1.4952597
View online: http://dx.doi.org/10.1063/1.4952597
View Table of Contents: http://scitation.aip.org/content/aip/journal/apl/108/21?ver=pdfcov
Published by the AIP Publishing

Time-resolved analysis of thickness-dependent dewetting and ablation of silver films upon nanosecond laser irradiation

Dongfeng Qi,[1,2,a)] Dongwoo Paeng,[1,a)] Junyeob Yeo,[1] Eunpa Kim,[1] Letian Wang,[1] Songyan Chen,[2] and Costas P. Grigoropoulos[1,b)]
[1]*Laser Thermal Laboratory, Department of Mechanical Engineering, University of California, Berkeley, California 94720-1740, USA*
[2]*Semiconductor Photonics Research Center, Department of Physics, Xiamen University, Xiamen 361005, People's Republic of China*

(Received 15 March 2016; accepted 13 May 2016; published online 25 May 2016)

Nanosecond pulsed laser dewetting and ablation of thin silver films is investigated by time-resolved imaging. Laser pulses of 532 nm wavelength and 5 ns temporal width are irradiated on silver films of different thicknesses (50 nm, 80 nm, and 350 nm). Below the ablation threshold, it is observed that the dewetting process does not conclude until 630 ns after the laser irradiation for all samples, forming droplet-like particles in the spot central region. At higher laser intensities, ablative material removal occurs in the spot center. Cylindrical rims are formed in the peripheral dewetting zone due to the solidification of transported matter at about 700 ns following the laser pulse exposure. In addition to these features, droplet fingers are superposed upon irradiation of 350-nm thick silver films with higher intensity. *Published by AIP Publishing.* [http://dx.doi.org/10.1063/1.4952597]

Arrays of micron- or nano-sized holes in metallic films exhibit local field enhancement, strong plasmonic response, and high electron emission.[1,2] During the last decade, such structures have attracted growing interest, owing to promising applications in optoelectronics[3,4] as well as other fields.[5]

Direct laser ablation and dewetting is an interesting method for machining holes in metallic specimens. Compared to conventional photolithography that is combined with reactive ion etching or chemical etching, nanosecond laser irradiation[6] has showed advantages in terms of its non-contact characteristics, low cost, and flexibility with respect to the target material. By tuning the incident laser power, it is possible to machine holes of different dimensions and shapes on metallic surfaces.[7]

Fundamental understanding of laser-induced dewetting and ablation processes is important in order to enable improved prediction and optimization of laser processes.[8,9] Several optical probing techniques have been developed for studying laser-material interactions.[10,11] For example, time-resolved shadowgraphy has been utilized to directly observe the ablation process in the nanosecond time regime,[12–14] capturing the ejected plume and shockwave emission at certain delay times.[15] Nevertheless, even in the simplest case of metal films, the induced phase change and the ensuing dewetting and ablation processes have not yet been fully investigated.

In this letter, time-resolved images revealed the evolution of different morphologies during the ablation and dewetting processes. We selected silver as the sample of interest because of its well-known properties and use as electrode material in electronics. Silver thin films of different thicknesses (50, 80, and 350 nm) were prepared by electron beam evaporation on quartz substrate. The time-resolved imaging system was set up as shown in Figure 1(a). Nd:YAG laser pulses of 532 nm wavelength and 5 ns temporal width impinged on silver film targets. The laser beam was focused by a 2× infinity corrected, non-achromatic long working distance objective lens at normal incidence. Nanosecond flash lamp (NANOLITE KL-K flash lamp, flash duration = 7 ns) was employed as an illumination source to provide temporally resolved images. These images were captured by a charge coupled device (CCD) camera via a 20× infinity objective lens. A digital delay generator was used to control the delay time between the processing laser and the image acquisition. The oscilloscope was used to record the actual delay time of the processing laser signal and the flash lamp signal. To ensure true representation, at least six images were examined at each delay setting.

We estimated the ablation threshold fluences of each film by linear curve fitting as shown in Figure 1(b). Above the ablation threshold fluence, F_{th}, the relationship between the ablated spot radius, r_a, and the laser fluence, F, is well characterized by a Gaussian beam profile, $r_a^2 = 2r_f^2[\ln(F) - \ln(F_{th})]$, where the $1/e$ beam radius,[16,17] r_f, is about 31 μm. If ${r_a}^2$ is plotted vs ln(F), extrapolation to ${r_a}^2 = 0$ yields the ablation threshold. For different thickness silver films (50, 80, and 350 nm), the ablation thresholds (F_{th}) were estimated as 0.92 J/cm^2, 2.59 J/cm^2, and 8.45 J/cm^2, respectively.

Next, we focus on investigating the surface morphologies produced by the exposure of the Ag films to near ablation threshold fluences. Figure 2(a) presents optical dark-field images, SEM images, and time-resolved images of the 50 nm Ag film surface. For low laser fluence below 0.89 J/cm^2, droplet-like structures are formed in the central area, implying melting and dewetting. As the fluence increases, the central droplet-like structures disappear, and melted material is dewetted radially outward. For the thicker samples (80 nm and 350 nm), as shown in Figures 2(b) and 2(c), droplet-like structures can also be formed

a)D. Qi and D. Paeng contributed equally to this work.
b)Author to whom correspondence should be addressed. Electronic mail: cgrigoro@berkeley.edu

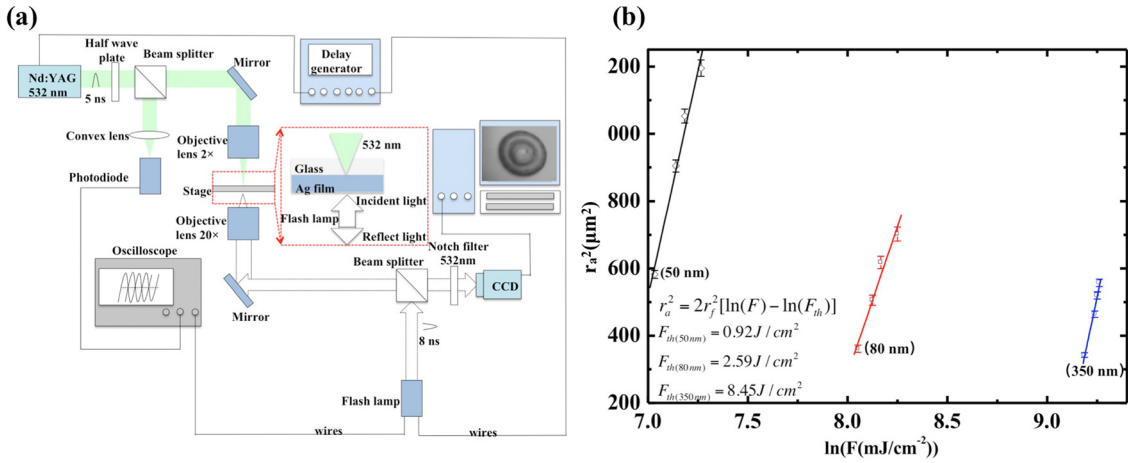

FIG. 1. (a) Time-resolved image setup of dewetting/ablation induced in silver by a excimer laser pulse with 5 ns duration, and the red frame is the magnified optical set-up image near the stage. (b) Squared radius of the ablation areas, r_a^2, with different silver thicknesses versus natural logarithm of the pulse fluence ln(F).

upon irradiation at fluences of 2.31 J/cm^2 and 7.71 J/cm^2, respectively. At higher laser fluences, peripheral rims and droplet fingers appear in the outskirts of the holes.

The transient evolution of the film surface morphologies at selected laser fluences are recorded using the time-resolved imaging setup and presented in Figure 3. As previously mentioned, micron-sized droplet-like particles are formed at lower laser fluences, i.e., around 0.89 J/cm^2 for the 50 nm film and 2.31 J/cm^2 for the 80 nm film. The time resolved images at the corresponding laser fluences in Figures 3(a) and 3(b) indicate that shiny small particles appeared in the central area of the irradiated zone at times of 200 ns and 500 ns after the laser irradiation, presumably formed by Ostwald ripening.[18] Furthermore, since micron-sized metallic particles of size parameter ($\chi = \pi D/\lambda$), where D is the particle diameter and λ the probing wavelength, scatter radiation strongly in the forward direction and yield much weaker back-scattering, the central area appears dark in reflection images beyond an elapsed time of 630 ns, signifying aggregation to bigger micron-sized particles. At slightly increased laser fluence, holes with droplet-like or cylindrical rim structures around these edges are formed on the silver film surface, respectively. At higher fluences, i.e., at and above 1.38 J/cm^2 for the 50 nm thickness specimen, the dewetted material is pulled toward the edges of the holes forming peripheral droplet-like structures after an elapsed time of 700 ns. For the 80 nm thick sample, rim structures can also be formed if the laser fluence is at or above 2.31 J/cm^2. For the 350 nm thick sample, several distinct stages in Figure 3(c) are observed at different laser fluences. Evidence of ablation in the center and dewetting in the edge area is observed at the laser fluence of 8.82 J/cm^2 that is slightly higher than the ablation threshold of 8.45 J/cm^2. At the higher laser fluences of 9.92 J/cm^2 and 10.52 J/cm^2, radially outward droplet fingers are observed.

Figures 4(a)–4(c) depict the SEM images of Ag thin films for different laser fluences, where the dewetting and ablation edges are distinct. Figure 4(d) gives the schematic

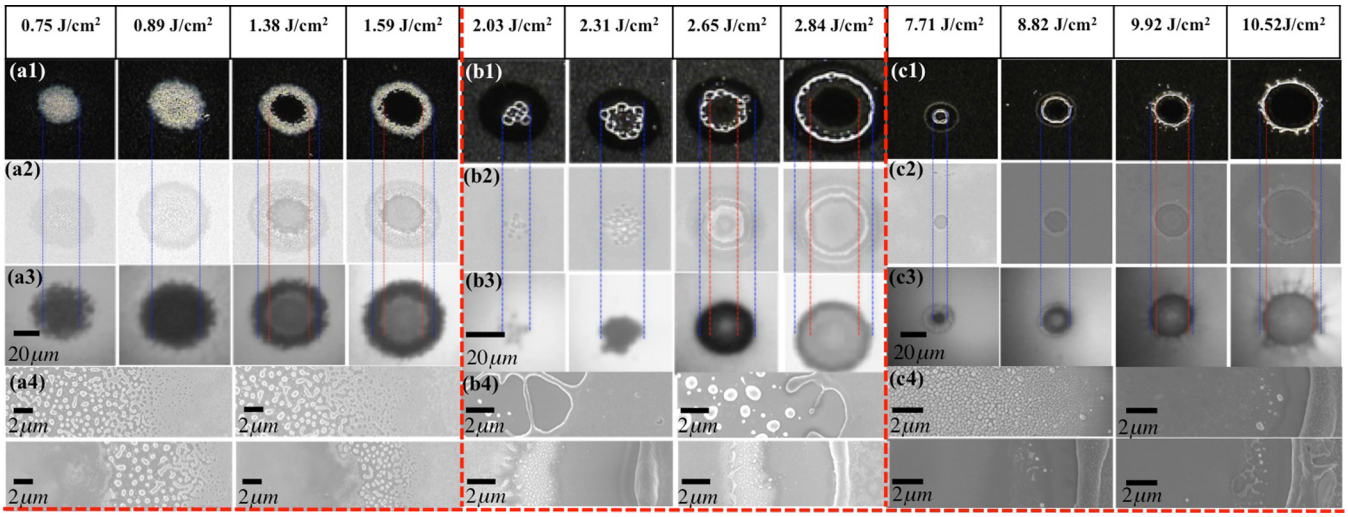

FIG. 2. Optical dark-field images (a1)–(c1), scanning electron microscopy (a2)–(c2), time-resolved images with 600 ns delayed (a3)–(c3), and the magnified SEM images (a4)–(c4) depict the characteristic stages of the morphological evolution of Ag film dewetting and ablation processing under different pulsed laser fluences. Figures (a4)–(c4) are corresponding magnified SEM images of figures (a2)–(c2) and give detailed information of edges between ablation and dewetting zones. (a) 50 nm thickness Ag film, (b) 80 nm thickness Ag film, and (c) 350 nm thickness Ag film. The red dashed lines mark the ablation edges and the blue dashed lines the dewetting edges of each sample.

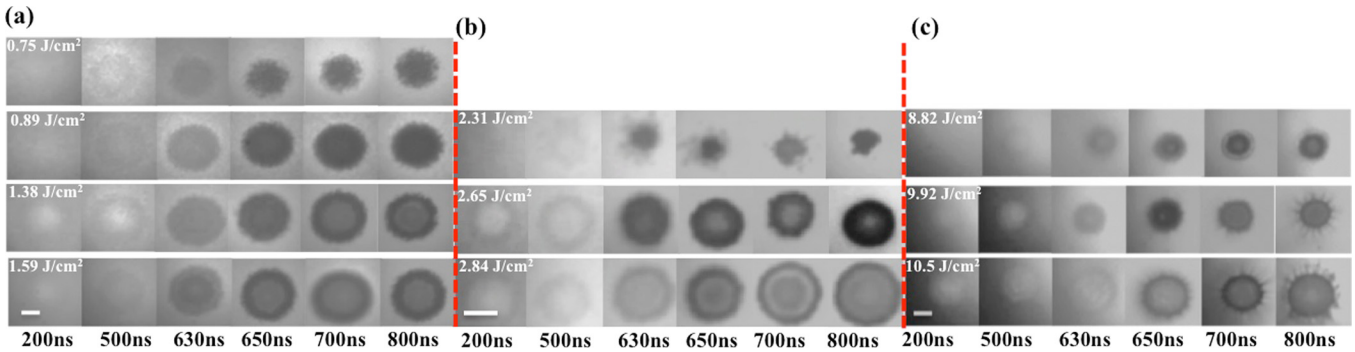

FIG. 3. Time-resolved image series of ns laser dewetting/ablation of silver films with different thicknesses: (a) 50 nm, (b) 80 nm, and (c) 350 nm. Each frame was taken at a certain flash lamp delay time. The scale bars in these images are all 20 μm.

diagram of ablation and dewetting distribution for 50 nm thickness sample under different laser fluences.[19] If the laser fluence (red curve) exceeds the ablation threshold, the central ablation area (blue line) surrounded by the dewetting zone (green line) appears. The dewetting regime (green line) solely appears in the spot center if the laser fluence (black curve) is below the ablation threshold.

Figure 5 depicts distinct stages of the thin film modification process and the corresponding ablation and dewetting threshold, respectively. If the laser intensity in the spot center is below the ablation threshold, in the dashed line region, the nanosecond laser pulse causes local dewetting of the Ag layer in the spot center.[20–22] In this case, nanoparticles grow larger through Ostwald ripening,[18] wherein the larger particles scavenge smaller ones, broadening the size distribution in the dewetting area after an elapsed time of 650 ns for all the samples (Figure 5(a)). If the laser fluence exceeds the respective ablation threshold of each sample, the SEM and time-resolved images of 50 nm sample show ablative material removal in the spot center and the formation of droplet-like particles in the peripheral dewetting zone after an elapsed time of 700 ns (Figure 5(b)). Rim structures are then formed in the 80 nm and 350 nm thick samples after laser irradiation (Figure 5(c)). It is recalled that the surface temperature is higher at the center of the melt pool, and the absorbed energy induces surface tension driven flow due to the high temperature gradient.[23] Consequently, due to the diminishing surface tension with increasing temperature for liquid metals, material should be transported radially outward by the positive surface tension gradient. However, the 50 nm film cannot supply significant mass transfer and only droplet-like particles are formed. Order of magnitude estimates[24] for the 50 nm film and melt pool diameter of 60 μm yield O(0.1 m/s) thermocapillary driven melt velocity that in turn corresponds to O(10^{-5} N) inertia force on the liquid pool. On the other hand, estimates of the recoil force exerted on the melt pool[24] for laser fluence in the range of 1 J/cm^2 yield O(10^{-1} N) values. Although the inertia force scales approximately with the square of the film thickness, it is still much smaller than the recoil force even for the 350 nm film. One may therefore expect that the thermal gradient driven surface flow is of minor consequence.[25–27] For the 350 nm thickness sample, as shown in Figure 5(d), the ablated splashed droplets shoot off the surface at higher laser fluence

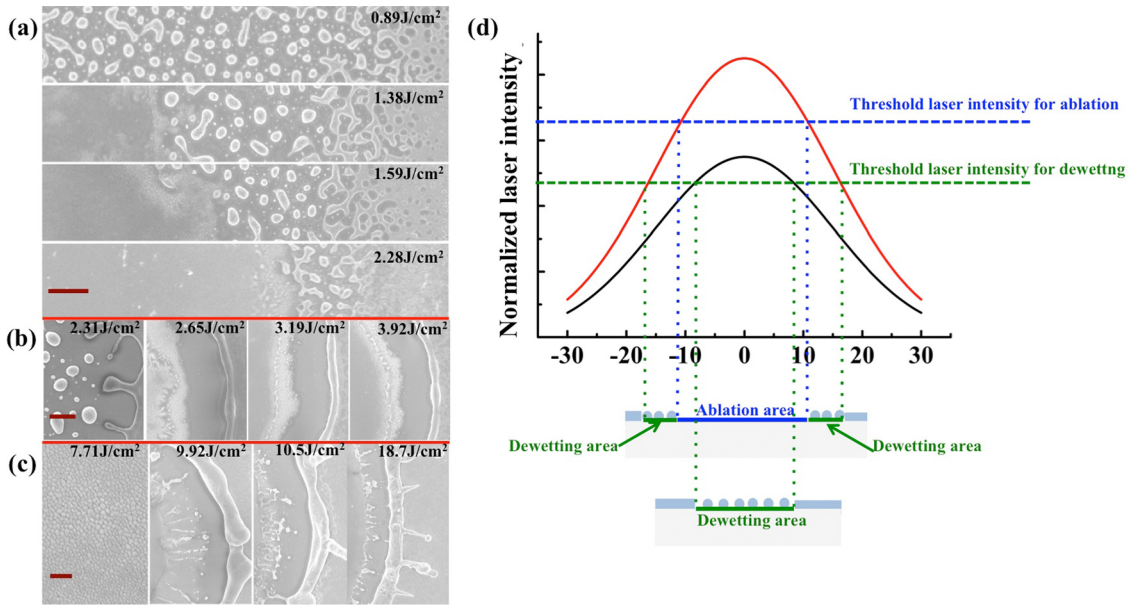

FIG. 4. Different surface morphologies of the Ag thin films with different laser fluences ((a) 50 nm, (b) 80 nm, and (c) 350 nm). (d) Normalized laser intensities of the ablation and dewetting threshold on the Ag thin film (50 nm) and corresponding ablation and dewetting line widths. Absorbed laser light intensities are normalized by the peak intensities of red curve. The scale bars in the SEM images are all 20 μm.

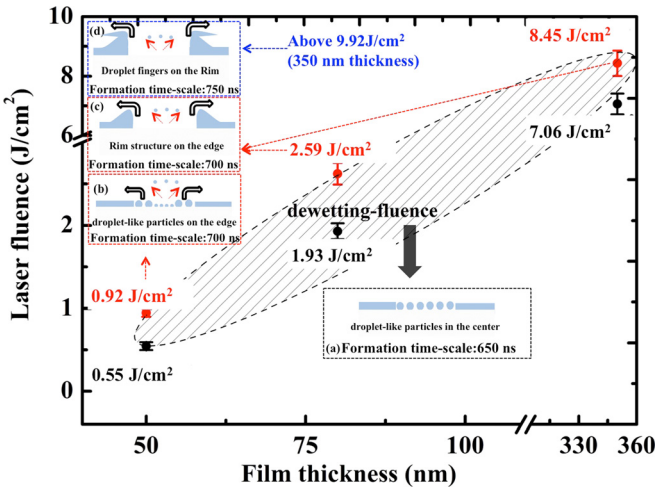

FIG. 5. The black and red labeled numbers are the dewetting and ablation thresholds, respectively. The insets (a)–(d) give a schematic illustration of mechanisms responsible for nanosecond laser-induced formation of surface structures on thin silver films. The dashed line region marks the dewetting fluences. Ablative material removal occurs for laser fluence exceeding the shaded area range. On the other hand, dewetting happens when the laser fluence is in the shade area. If the laser fluence is lower than the dewetting threshold, no surface morphology changes are observed.

(above 9.92 J/cm^2), exerting strong recoil force and producing droplet fingers (Figure 5(d)). For higher laser fluence, the liquid Ag materials are squeezed out of the pool very quickly by the diminishing surface tension and pushed around the peripheral rim structure. Droplet fingers occur due to the recoil force induced acceleration around the rim.[23,26,27] The same experimental trends would be observed in thin films of different inorganic materials and comparable thickness. The effect of the wavelength is not particularly significant for the present experiments, as it affects merely the magnitude of the energy input into the film. However, the laser interaction with the ejected matter would depend on the laser wavelength. This is likely to be important at the higher fluences where the ablation is accompanied by the plasma effects and the problem becomes more strongly coupled due to the fluid dynamics and radiative transport in the ejected plume.

In conclusion, we have carried out *in-situ* visualization of nanosecond laser-induced dewetting and ablation processes in thin silver films. The time-resolved imaging setup helped elucidate the transient breakup of the dewetted melt pool, the surface tension induced mass transport, and the effect of the ablative material removal and their dependence on the imparted laser fluence.

D. F. Qi acknowledges the support of the Chinese Scholars Council and the National Science Foundation of China (Grant Nos. 61474081 and 61534005).

[1]J. A. Schuller, E. S. Barnard, W. S. Cai, Y. C. Jun, J. S. White, and M. L. Brongersma, Nat. Mater. **9**, 193 (2010).
[2]C. C. Chang, Y. D. Sharma, Y. S. Kim, J. A. Bur, R. V. Shenoi, S. Krishna, D. H. Huang, and S. Y. Lin, Nano Lett. **10**, 1704 (2010).
[3]C. Genet and T. W. Ebbesen, Nature **445**, 39 (2007).
[4]D. W. Paeng, J. H. Yoo, J. Y. Yeo, D. Lee, E. Kim, S. H. Ko, and C. P. Grigoropoulos, Adv. Mater. **27**, 2762 (2015).
[5]A. D. Wang, L. Jiang, X. W. Li, Y. Liu, X. Z. Dong, L. T. Qu, X. M. Duan, and Y. F. Lu, Adv. Mater. **27**, 6238 (2015).
[6]J. Siegel, D. Puerto, W. Gawelda, G. Bachelier, and J. Solis, Appl. Phys. Lett. **91**, 082902 (2007).
[7]D. F. Qi, H. H. Liu, W. Gao, S. Y. Chen, C. Li, H. K. Lai, W. Huang, and J. Li, Opt. Express **21**(8), 9923 (2013).
[8]D. J. Hwang, C. P. Grigoropoulos, J. Yoo, and R. E. Russo, Appl. Phys. Lett. **89**, 254101 (2006).
[9]D. J. Hwang, H. J. Jeon, C. P. Grigoropoulos, J. Yoo, and R. E. Russo, Appl. Phys. Lett. **91**, 251118 (2007).
[10]D. W. Paeng, D. H. Lee, J. Y. Yeo, J. H. Yoo, F. I. Allen, E. Kim, H. Y. So, H. K. Park, A. M. Minor, and C. P. Grigoropoulos, J. Phys. Chem. C **119**(11), 6363 (2015).
[11]D. W. Paeng, D. H. Lee, and C. P. Grigoropoulos, Appl. Phys. Lett. **105**, 073110 (2014).
[12]J. H. Yoo, S. H. Jeong, R. Greif, and R. E. Russo, J. Appl. Phys. **88**, 1638 (2000).
[13]A. D. Giacomo, M. Dell'Aglio, A. Santagata, R. Gaudiuso, O. De Pascale, P. Wagener, G. C. Messina, G. Compagninie, and S. Barcikowskid, Phys. Chem. Chem. Phys. **15**, 3083 (2013).
[14]D. G. Papazoglou, A. Karaiskou, I. Zergioti, and C. Fotakis, Appl. Phys. Lett. **81**, 1594 (2002).
[15]C. Porneala and D. A. Willis, Appl. Phys. Lett. **89**, 211121 (2006).
[16]J. Jandeleit, G. Urbasch, H. Hoffmann, H. G. Treusch, and E. Kreutz, Appl. Phys. A **63**, 117 (1996).
[17]C. P. Grigoropoulos, *Transport in Laser Microfabrication: Fundamentals and Applications* (Cambridge University Press, Cambridge, 2009).
[18]P. L. Redmond, A. J. Hallock, and L. E. Brus, Nano Lett. **5**(1), 131 (2005).
[19]D. W. Paeng, J. Y. Yeo, D. Lee, E. Kim, S. J. Moon, and C. P. Grigoropoulos, Appl. Phys. A **120**, 1229 (2015).
[20]Y. Wu, J. D. Fowlkes, and P. D. Rack, J. Mater. Res. **26**(2), 277 (2011).
[21]Y. N. Kulchin, O. B. Vitrik, A. A. Kuchmizhak, V. I. Emel'yanov, A. A. Ionin, S. I. Kudryashov, and S. V. Makarov, Phys. Rev. E **90**, 023017 (2014).
[22]H. Krishna, N. Shirato, C. Favazza, and R. Kalyanaraman, J. Mater. Res. **26**(2), 154 (2011).
[23]R. Hergenröder, Spectrochim. Acta, Part B **61**, 284 (2006).
[24]D. Bäuerle, *Laser Processing and Chemistry*, 4th ed. (Springer, Heidelberg, 2011), pp. 191, 217.
[25]I. Egry, E. Ricci, R. Novakovic, and S. Ozawa, Adv. Colloid Interface Sci. **159**, 198 (2010).
[26]G. D. Tsibidis, M. Barberoglou, P. A. Loukakos, E. Stratakis, and C. Fotakis, Phys. Rev. E **86**, 115316 (2012).
[27]J. Mazumder, Opt. Eng. **30**(8), 1208 (1991).